Published online 6 September 2023 *Nucleic Acids Research, 2023, Vol. 51, No. 18* **9905–9919**
https://doi.org/10.1093/nar/gkad725

Genome-wide screening reveals metabolic regulation of stop-codon readthrough by cyclic AMP

Zhihui Lyu[1], Patricia Villanueva[1], Liam O'Malley[1], Parker Murphy[1], Jacques Augenstreich[1], Volker Briken[1], Abhyudai Singh[2] and Jiqiang Ling[1,*]

[1]Department of Cell Biology and Molecular Genetics, The University of Maryland, College Park, MD, USA and [2]Department of Electrical and Computer Engineering and Biomedical Engineering, University of Delaware, Newark, DE, USA

Received July 20, 2023; Revised August 12, 2023; Editorial Decision August 14, 2023; Accepted August 21, 2023

ABSTRACT

Translational fidelity is critical for microbial fitness, survival and stress responses. Much remains unknown about the genetic and environmental control of translational fidelity and its single-cell heterogeneity. In this study, we used a high-throughput fluorescence-based assay to screen a knock-out library of *Escherichia coli* and identified over 20 genes critical for stop-codon readthrough. Most of these identified genes were not previously known to affect translational fidelity. Intriguingly, we show that several genes controlling metabolism, including *cyaA* and *crp*, enhance stop-codon readthrough. CyaA catalyzes the synthesis of cyclic adenosine monophosphate (cAMP). Combining RNA sequencing, metabolomics and biochemical analyses, we show that deleting *cyaA* impairs amino acid catabolism and production of ATP, thus repressing the transcription of rRNAs and tRNAs to decrease readthrough. Single-cell analyses further show that cAMP is a major driver of heterogeneity in stop-codon readthrough and rRNA expression. Our results highlight that carbon metabolism is tightly coupled with stop-codon readthrough.

GRAPHICAL ABSTRACT

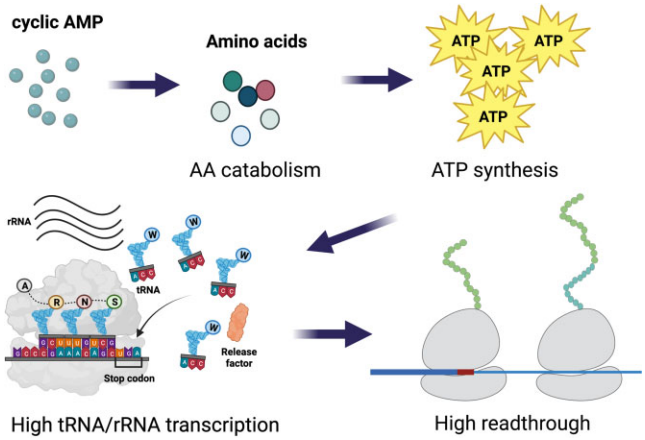

INTRODUCTION

Accurate translation of mRNA into proteins is a central and delicately controlled cellular process (1–4). Aminoacyl-tRNA synthetases (aaRSs) are challenged to ligate the correct amino acids to the tRNAs (5). Given the similarity between amino acids, an editing step is used by approximately half of the aaRSs to remove misactivated amino acids or mismatched aminoacyl-tRNAs (aa-tRNAs) (2,6,7). The accurate pairing of the resulting aa-tRNAs to the mRNA codons on the ribosome also needs kinetic proofreading (8). Despite such conserved quality control mechanisms, base levels of translational errors remain high compared with DNA replication and transcription (9). The amino acid misincorporation rate at sense codons is approximately 10^{-4} to 10^{-3}, and the frequency of stop-codon readthrough is even higher at 10^{-3} to 10^{-2} (10–14). It is important to note that such error rates are not fixed and can fluctuate due to mutations, mRNA context and environmental changes (2,15–19). Mutations in aaRSs and tRNAs may lead to the production of misacylated tRNAs, which are

*To whom correspondence should be addressed. Tel: +1 301 405 1035; Email: jling12@umd.edu

used by the ribosome to make erroneous proteins (4,7,20–23). Recent studies suggest that some tRNA variants in human populations lead to increased translational errors and may function as disease modifiers (19,24). Mutations in ribosomal proteins and RNAs also affect the decoding accuracy to cause amino acid misincorporation, stop-codon readthrough and frameshift (13,25,26). Further, programmed stop-codon readthrough and frameshift are frequently used by viruses and host cells to regulate the expression of alternative protein variants (27,28). In addition to genetic changes, environmental cues can also affect various types of translational errors. For example, oxidative stress impairs the editing function of threonyl-tRNA synthetase and causes serine misincorporation at threonine codons in *Escherichia coli* (29). Conversely, oxidation of phenylalanyl-tRNA synthetase enhances editing and confers hyper accuracy (18). It has also been shown that acid stress increases stop-codon readthrough on the ribosome by compromising the activity of release factors (16).

Reduced translational fidelity often leads to detrimental effects such as slow growth, cell death and neurological disorders (30). Recent studies in yeasts, flies, worms, and mice demonstrate that increasing translational fidelity by a ribosomal mutation improves the life span, whereas decreasing translational fidelity leads to accelerated aging (31,32). However, maintaining high fidelity also comes with costs, and translational errors have been shown to be beneficial under certain conditions, particularly during microbial stress responses and host interactions (33). For example, increasing ribosomal decoding fidelity decreases resistance to oxidative stress in *E. coli* and the expression of virulence genes in *Salmonella enterica* (34,35). Elevating amino acid misincorporation also increases resistance against antibiotics in *Mycobacteria* (36,37).

Despite decades of work, the genetic factors and pathways that regulate translational fidelity are still not fully understood. Strikingly, although translational errors have been shown to fluctuate among single cells in genetically-identical populations of bacteria (14,36), what drives such heterogeneity in translational errors remains completely unknown. In this study, we used recently developed dual-fluorescence reporters to perform high-throughput screening of the *E. coli* knockout library. In addition to a few genes that were previously shown to affect translational fidelity (e.g. *miaA* and *prfC*), we identified over 20 novel genes that either increase or decrease stop-codon readthrough. The effects of the identified genes on translational fidelity were then validated by testing reporters and native stop codons in *E. coli* deletion mutants that were independently constructed. Our screening revealed several interesting metabolic genes that regulate translational fidelity. Further mechanistic studies show that cAMP promotes amino acid catabolism and ATP production to enhance the transcription of tRNAs and stop-codon readthrough. We also show that in single cells, fluctuation of the cAMP level promotes noise in stop-codon readthrough and rRNA expression. This work thus revealed a central role of cAMP in coupling carbon metabolism with stop-codon readthrough and ribosome biogenesis, as well as driving the heterogeneity of translational errors among single cells.

MATERIALS AND METHODS

Bacterial strains, plasmids, growth conditions and reagents

All strains and plasmids used in this study are listed in Table S4. The oligonucleotides used for gene disruption and plasmid construction are listed in Table S5. Gene knockout was performed as described (38). Unless otherwise noted, all bacteria used in this study were cultured in regular LB consisting of 10 g/l tryptone, 5 g/l sodium chloride and 5 g/l yeast extract at 25°C or 37°C. The composition of M9 medium was 47.8 mM Na_2HPO_4, 22.0 mM KH_2PO_4, 18.7 mM $(NH4)_2SO_4$, 8.6 mM NaCl, 2.0 mM $MgSO_4$, 0.1 mM $CaCl_2$ and 0.40% glucose with or without supplementation of 40 mM tryptophan. The concentrations of antibiotics used were as follows: 100 μg/ml ampicillin (Amp), 25 μg/ml chloramphenicol (Chl) and 50 μg/ml kanamycin (Kan). 10 mM arabinose was added for the induction of the lambda Red recombinase on pKD46.

Plasmid transformation

For the initial screening, plasmids were transformed into the Keio collection in 96-well plates. Cells were grown at 37°C in 100 μl LB per well to mid-log phase and centrifuged at 4000 g for 10 min. Each pellet was resuspended in 20 μl fresh transformation buffer (LB broth with 10% polyethylene glycol (PEG3350), 5% dimethyl sulfoxide (DMSO), 10 mM $MgSO_4$ and 10 mM $MgCl_2$). 20 μl KCM buffer (0.1 M KCl, 0.03 M $CaCl_2$ and 0.05 M $MgCl_2$) with ∼10 ng plasmid was added to the competent cells, followed by 30 min of incubation on ice. The cell/DNA mixture was placed at room temperature for 10 min before the addition of 40 μl LB pre-warmed at 37°C. The cells were then incubated at 37°C with shaking for 1 h. 80 μl LB with 200 μg/ml Amp was added to each well to select the transformants. After overnight incubation at 37°C, the cultures were diluted 1:50 in LB with 100 μg/ml Amp and incubated at 37°C with shaking to saturation.

Fluorescence-based stop-codon readthrough assay

Stop-codon readthrough rates were determined as described (14). Briefly, overnight cultures of *E. coli* were diluted 1:50 in LB or M9 and incubated at 25°C or 37°C using 96-well black side plates with a clear bottom (Corning). After 16 h, the fluorescence intensity of mCherry and YFP was determined in a microplate reader (Synergy HTX, BioTek). The level of stop-codon readthrough was calculated by determining the YFP/mCherry ratio of pZS-P*tet*-m-TGA-y relative to the YFP/mCherry ratio of the control pZS-P*tet*-m-y, and pZS-P*tet*-lacZ was used as for background subtraction. When necessary, 4 mM cyclic-AMP or 2 μg/ml Chl was added into the culture.

Dual luciferase assay

Cells grown at 37°C to mid-log phase in LB supplemented with 100 μg/ml ampicillin were pelleted, washed once with phosphate-buffered saline (PBS) and lysed in 50 μl passive lysis buffer (PLB). After incubation at room temperature for 15 min, the samples were flash-frozen in liquid nitrogen

and then thawed on ice. Firefly and Renilla luciferase activities were determined using the Dual-Luciferase Reporter Assay System (Promega) according to the manufacturer's instruction, and the error frequencies were determined as previously described (10).

Western blot analysis

Overnight cultures of *E. coli* were diluted 1:50 in LB and grown aerobically at 37°C with vigorous shaking to mid-log phase. *E. coli* strains containing pFLAG-MAC-NudL were induced with 1 mM IPTG for another 2 h. The total cell protein was harvested using trichloroacetic acid TCA precipitation. Total proteins were quantified by bicinchoninic acid (BCA) assay before being separated on 10% SDS-PAGE and transferred onto nitrocellulose membranes via wet transfer then blocked in tris-buffered saline with Tween 20 (TBST) containing 5% non-fat milk. The levels of readthrough NudL and RF2 were probed by an anti-FLAG primary antibody at a dilution of 1:1000. The level of EF-Tu protein was probed by an anti- EF-Tu antibody at a 1:300 dilution and a secondary anti-mouse IgG antibody at a dilution of 1:10 000. Signals were detected by the Clarity Western ECL Substrate in the ChemiDoc Imaging System (Bio-Rad). Ponceau Red staining was performed as a loading control.

Single-cell UGA readthrough using fluorescence microscopy

Overnight cultures of *E. coli* carrying the pZS-P*tet*-mCherry-TGA-y plasmid were diluted 1:50 in LB and grown aerobically at 25°C for 16 h with shaking. 3 μl of the resulting cultures were placed on a 1.5% agarose LB pad on a single slide. Fluorescence images were obtained using BZ-X800 fluorescence microscope (Keyence) with a 100× oil lens. For single bacterial fluorescence analysis, bacteria were segmented using both the cloud-based segmentation software APEER (39) and Cellpose deep-learning segmentation software (40,41). For the segmentation using APEER, a model was trained for instance segmentation using five representative images in the mCherry channel from the experiment datasets. After the training, the entire dataset was segmented. The generated mask images were then used to generate Regions Of Interest (ROIs) in Fiji (NIH) using a custom-made macro. Briefly, the mask images were analyzed using the 'find edges' function, then a threshold was applied to create a binary image. Next, the 'Analyze particles' function was used to detect bacteria and draw ROIs. These ROIs were finally used on the different channels of the raw images to measure the mean fluorescence intensity values of individual bacteria. For the segmentation using Cellpose, models were trained using representative images in the mCherry channel from different experiments. The training models were generated using representative images of the different experiments. The segmentation was then performed on the datasets using a notebook on the jupyter-lab software. The ROIs were then drawn on Fiji using the text file given after segmentation for each image and the Python script as described in the Cellpose tutorial. The created ROIs were then applied on every channel of the raw images to measure the mean fluorescence intensity values of individual bacteria. The code used for single bacterial fluorescence analysis is available via GitHub at https://github.com/MouseLand/cellpose.

Measurements of promoter activity with a platereader

Overnight cultures were diluted 1:50 and grown in LB at 25°C or 37°C with vigorous shaking. After 16 h, the fluorescence was measured using the microplate reader 3 (Synergy HTX, BioTek) as follows: mCherry (excitation wavelength at 575 nm and emission wavelength at 620 nm), and eCFP (excitation wavelength at 420 nm and emission wavelength at 475 nm). The gain was set manually to 40. The promoter activity was calculated as the ratio of eCFP over mCherry.

RNA sequencing

Overnight cultures were diluted 1:50 and grown in LB at 37°C with vigorous shaking to mid-log phase. Total RNAs were extracted using the RNAeasy kit according to the manufacturer's protocol (Qiagen), and Illumina RNA sequencing was performed by Genewiz. Sequence reads were trimmed to remove possible adapter sequences and nucleotides with poor quality using Trimmomatic v.0.36. The trimmed reads were then mapped to the e_coli_MG1655_NCBI reference genome available on ENSEMBL using the Bowtie2 aligner v.2.2.6. Unique gene hit counts were calculated by using featureCounts from the Subread package v.1.5.2. The hit counts were summarized and reported using the locus_tag feature in the annotation file. Only unique reads that fell within gene regions were counted. Since a strand-specific library preparation was performed, the reads were strand-specifically counted.

Metabolomics analysis

Overnight cultures were diluted 1:50 and grown in LB at 37°C with vigorous shaking to mid-log phase, and amino acid metabolomics analysis was performed by Metabolon, Inc. Cell pellet samples were analyzed for twenty-two amino acids: Alanine, Arginine, Asparagine, Aspartic acid, Glutamic acid, Glutamine, Glycine, Histidine, Isoleucine, Leucine, Lysine, Methionine, Phenylalanine, Proline, Serine, Threonine, Tryptophan, Tyrosine, Valine, trans-4-Hydroxyproline, Ornithine and Citrulline by LC–MS/MS according to the Metabolon Method TAM146. Samples were analyzed with the Agilent 1290/AB Sciex QTrap 5500 LC–MS/MS system equipped with a C18 reversed-phase UHPLC column. The mass spectrometer was operated in positive mode using electrospray ionization (ESI). The peak areas of the individual analyte parent ions were measured against the peak areas of the parent ions of the corresponding internal standards in pseudo-MRM mode. Quantitation was performed using a weighted least squares regression analysis generated from fortified calibration standards prepared immediately prior to each run. LC–MS/MS raw data were collected and processed using SCIEX OS-MQ software v3.0. Data reduction was performed using Microsoft Excel for Office 365 v.16.

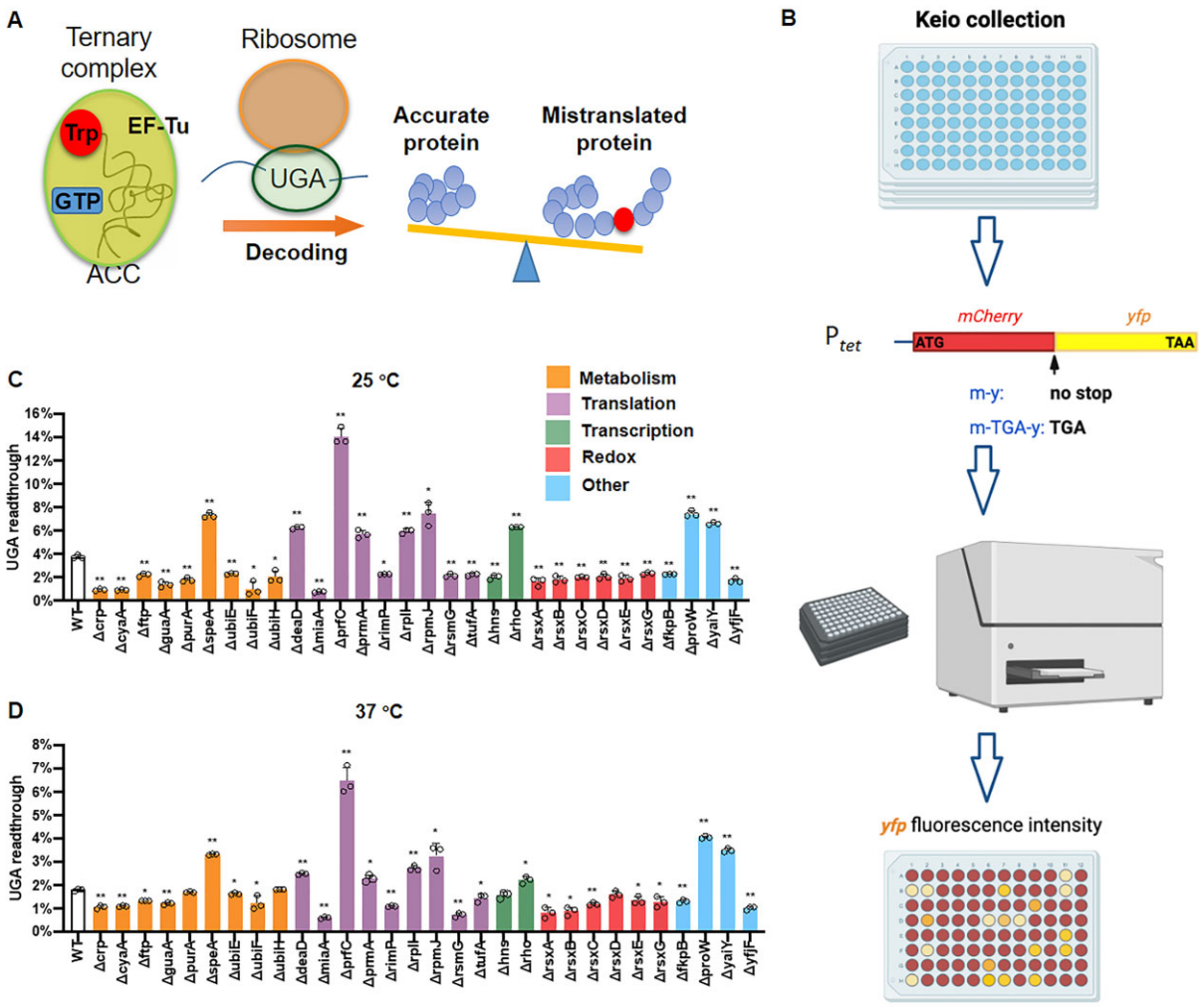

Figure 1. Genome-wide screening of *E. coli* knockout library reveals genetic control of UGA readthrough. (**A**) The EF-Tu:Trp-tRNA^{Trp}:GTP ternary complex competes with release factor 2 (RF2) to suppress the UGA stop codon and produce extended proteins. (**B**) Workflow of high-throughput screening for *E. coli* knockout mutants with altered UGA readthrough. The plasmids carrying the UGA readthrough reporter (pZS-P*tet*-m-TGA-y) and the control (pZS-P*tet*-m-y) were transformed into the Keio knockout collection using 96-well plates. The transformants were then cultured and measured for fluorescence intensity in a platereader. (C, D) Overnight cultures of *E. coli* variants with pZS-P*tet*-m-TGA-y and pZS-P*tet*-m-y were diluted 1:50 in fresh LB Amp over 16 h at 25 (**C**) and 37°C (**D**), respectively. The fluorescence intensity of mCherry and YFP was determined using a platereader. UGA readthrough rates were calculated using the normalized ratio of YFP over mCherry. Error bars indicate standard deviations. *P* values were calculated using the unpaired t-test comparing the mutants with the WT. * $P \leq 0.05$, ** $P \leq 0.01$. Figure 1B was created with BioRender.com.

RNA/protein ratio assay

The measurement of RNA/protein ratios was adapted from You *et al.* (42). Briefly, cells were grown at 25°C or 37°C to the mid-log phase in LB with shaking. 1.5 ml culture was collected by centrifugation, and the cell pellet was fast-frozen in liquid nitrogen. For the total RNA quantification, the pellet was first washed twice with 0.7 M $HClO_4$ and digested with 0.3 M KOH for 1 h at 37°C with occasional mixing. The cell extract was further neutralized with 0.1 ml of 3 M $HClO_4$, and the supernatant was collected. The precipitate was re-extracted twice with 0.55 ml of 0.5 M $HClO_4$ and a final volume of 1.5-ml supernatant was combined. The total RNA concentration was determined in a microplate reader Take 3 (Synergy HTX, BioTek). For quantification of total proteins, the thawed cell pellet was digested with 100 μl of 3 M NaOH and heated at 98°C for 5 min before cooling down to room temperature. The Biuret reaction was carried out by adding 100 μl of 1.6% $CuSO_4$ to the above cell mixture with thorough mixing and incubating at room temperature for 5 min. The reaction mixture was centrifuged at 13 000 g for 1 min and the supernatant was measured for its absorbance at 555 nm. A similar experimental process was applied to a series of bovine serum albumin (BSA) standards to obtain a standard curve.

Northern blot analysis

The total RNA was isolated from 1 ml mid-log phase cultures using TRIzol® Reagent (Invitrogen). The resulting lysate was phase separated with 200 μl chloroform and the total RNA was precipitated with the same volume of ice-cold isopropanol. The pellet was washed twice with 75%

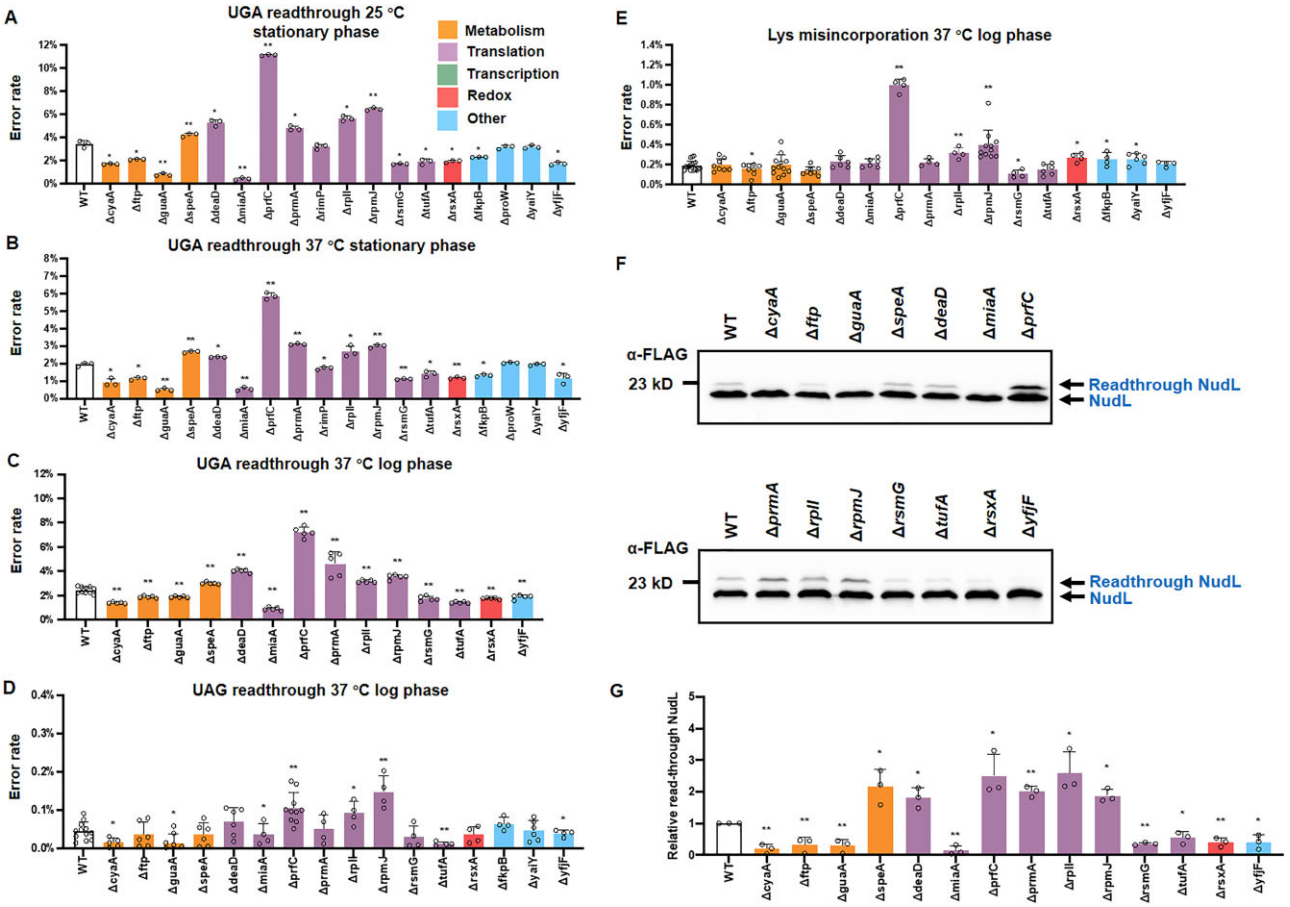

Figure 2. Error rates of mutants derived from MG1655. (A–C) UGA readthrough reporter (pZS-P*tet*-m-TGA-y) and the control (pZS-P*tet*-m-y) plasmids were transformed into *E. coli* MG1655 WT and mutant strains. Overnight cultures of *E. coli* were diluted 1:50 in LB Amp and incubated for 16 h to the stationary phase (**A, B**) or the mid-log phase (**C**). UAG readthrough (**D**) and lysine misincorporation (**E**) rates were determined using dual-luciferase reporters. (**F**) Readthrough of a native UGA codon in *nudL* with an N-terminal FLAG tag in *E. coli* variants grown in LB at 37°C. UGA readthrough yields a longer NudL protein variant, as shown by western blot. (**G**) Quantitation of readthrough levels in (F). The trend of UGA readthrough changes in the mutants in (G) is the same as in (C). Error bars indicate standard deviations. *P* values were calculated using the unpaired *t*-test comparing the mutants with the WT. * $P \leq 0.05$, ** $P \leq 0.01$.

ethanol and resuspended in 30–50 μl of nuclease-free water by incubating at room temperature for 20 min. 3 μg total RNA was separated by electrophoresis on a vertical 8% (w/v) polyacrylamide gel with 8 M urea in Tris–borate–EDTA (TBE) buffer at 120 V for 3 h. The samples were then transferred to the Zeta-Probe nylon membrane (Bio-Rad), cross-linked by UV light exposure and hybridized with oligonucleotide probes labeled with biotin at the 5′ end (see Table S5) at 42°C. The $tRNA^{Trp}$ signal was normalized to the signal of the loading control SsrA RNA by using ImageJ (The National Institutes of Health). For acidic-gel norther blot, the pellet was resuspended in 30–50 μl of gel loading buffer (10 mM sodium acetate, pH 5.0 and 1 mM EDTA) and incubated at room temperature for 20 min. Acid urea polyacrylamide gel electrophoresis was performed as previously described in Fan *et al.* (14). Briefly, each acidic urea polyacrylamide gel was made with 10% polyacrylamide, 8 M urea and 0.1 M sodium acetate, pH 5.0 and 3 μg of RNA sample was loaded onto the gel, and run at 90 V at 4°C for 15–18 h. The later steps following electrophoresis were performed as described above.

Determination of growth rate

E. coli cells were diluted 1:100 into fresh LB and incubated at 25°C or 37°C for 16 h with shaking. Cell growth was automatically monitored every 20 min by measuring the optical density at 600 nm (A_{600}) using a microplate reader (Synergy HTX, BioTek). The growth rates were obtained from the exponential growth phase.

Intracellular ATP detection

Cells were grown at 37°C in LB to mid-log phase and were normalized by A_{600}. 1 ml culture aliquot was washed once with ice-cold PBS and resuspended in 300 μl of the same buffer. The ATP level was measured using an ATP Determination Kit (Invitrogen) according to the manufacturer's instructions. Blank PBS was used for background subtraction.

Flow cytometry

Cells harboring pZS-P*tet*-eCFP-TGA-y plasmid were grown in fresh LB aerobically for 16 h at 25°C with

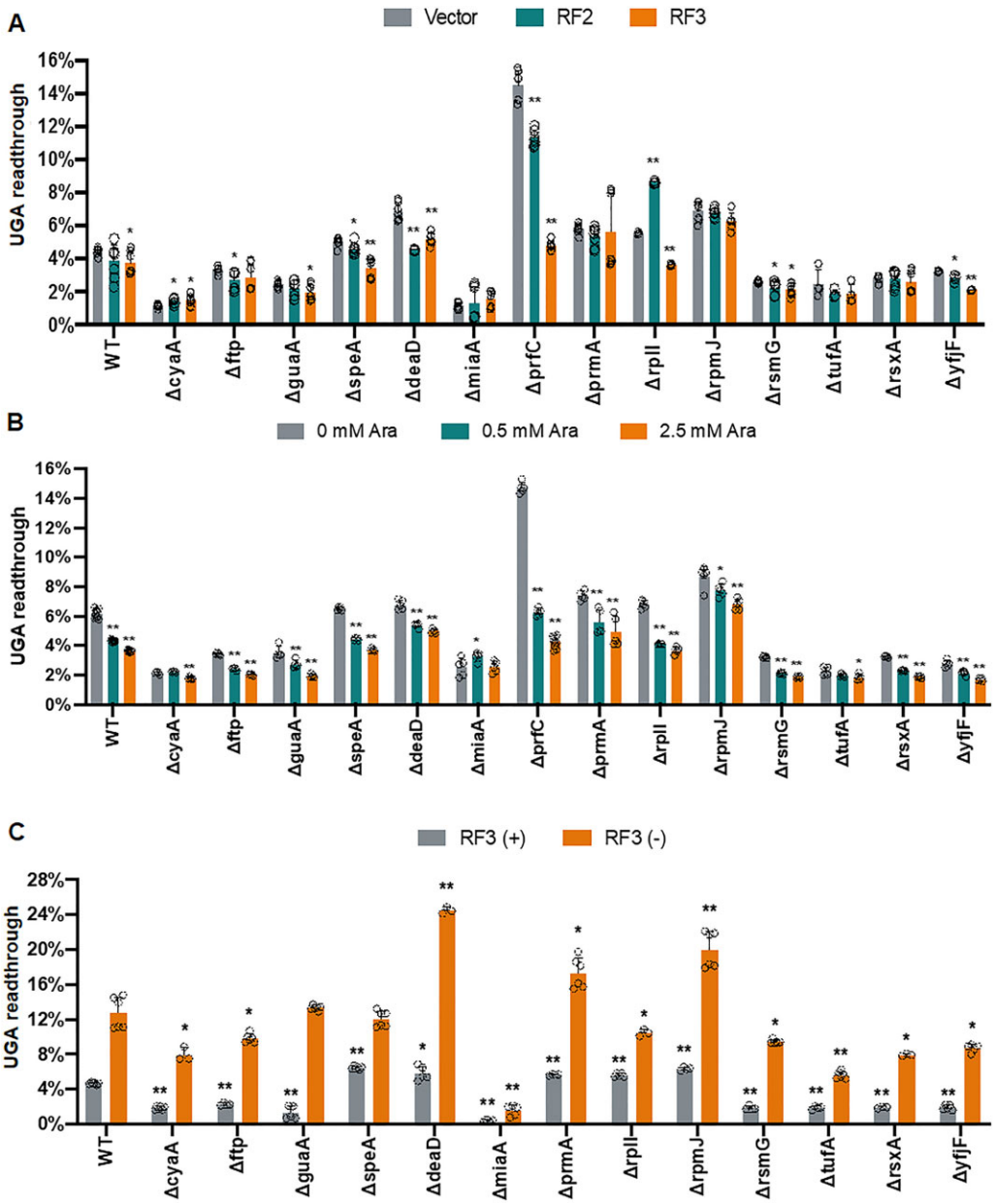

Figure 3. Effects of release factors on UGA readthrough in *E. coli* mutants. (**A**) ASKA plasmids expressing RF2 or RF3 were transformed into *E. coli* variants with pZS-P*tet*-m-TGA-y and pZS-P*tet*-m-y. The UGA readthrough levels were determined as in Figure 1. The same strains expressing RF2 or RF3 were compared with those carrying the empty ASKA vector. (**B**) Strains expressing RF2 from ASKA and RF3 from pKT under the pBAD promoter induced by arabinose. The strains grown in the presence of arabinose were compared with the same strains grown without arabinose. (**C**) UGA readthrough in the presence and absence of RF3. The mutant strains were compared with the WT with or without RF3. Error bars indicate standard deviations. *P* values were calculated using the unpaired *t*-test. * $P \leq 0.05$, ** $P \leq 0.01$.

shaking, diluted in PBS with 25 μg/ml Chl, and kept at 4°C before flow cytometry on BD FACSCanto II flow cytometer. 30 000 gated events were collected for each sample and FlowJo software was used for further data analysis.

Analyses of CV and noise

We consider a simple model where single-cell fluctuations in cAMP levels impacts P*rrsC* activity, and fluctuations in the promoter activity propagate to determine UGA readthrough. CV was calculated as the ratio of standard deviation and mean as previously described (14,43).

The cAMP-dependence of noise in the P*rrsC* activity and UGA readthrough was dissected by decomposing its CV as follows:

$$CV^2 = CV^2_{cAMP} + CV^2_{other}$$

$CV_{cAMP}{}^2$ represents the noise contribution from cAMP, and $CV_{other}{}^2$ is the contribution from other factors impacting P*rrsC* activity (eCFP/mCherry in Figure 7B) or UGA readthrough (YFP/mCherry in Figure 7B). The noise con-

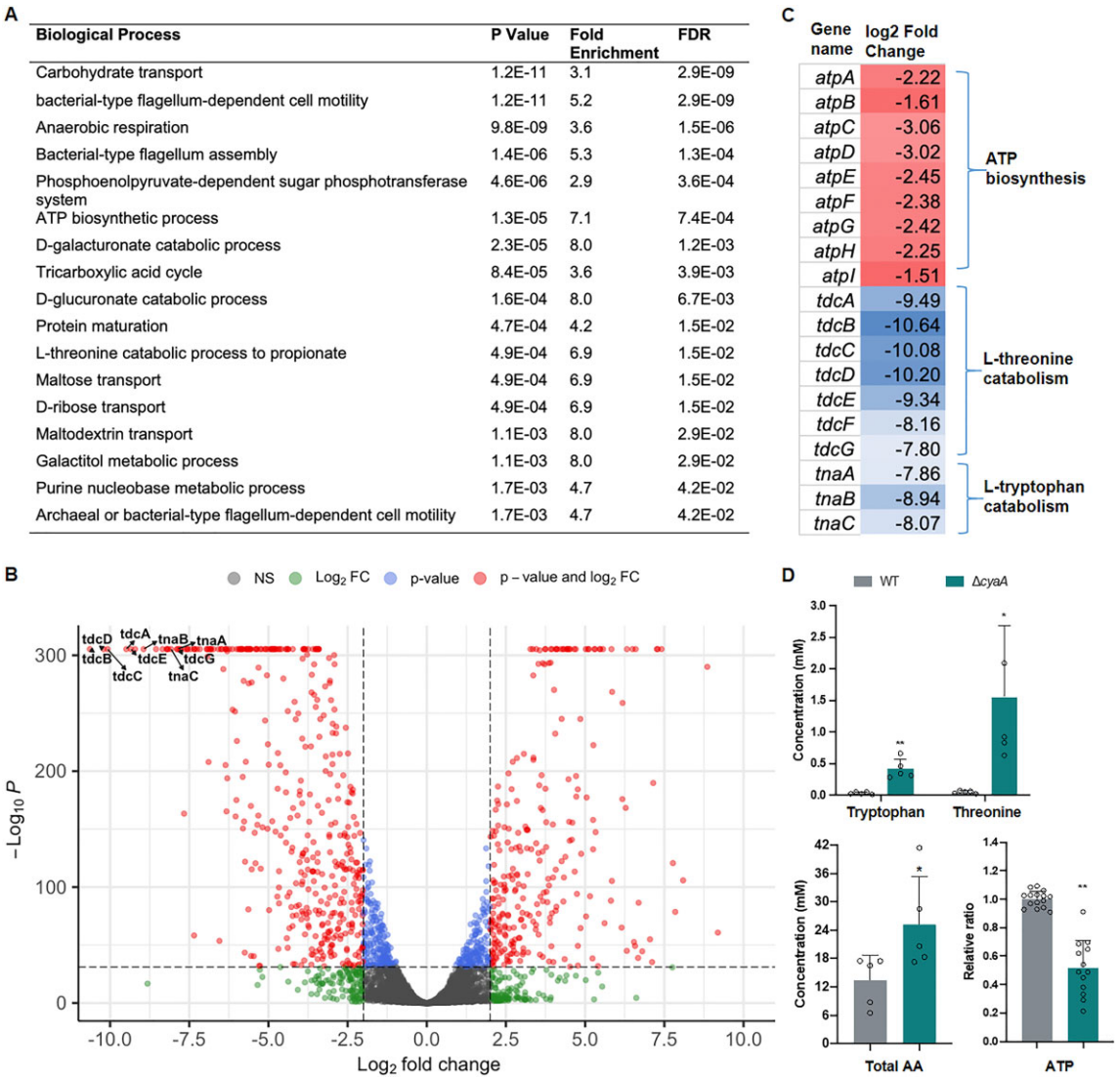

Figure 4. RNA sequencing and metabolic analyses of Δ*cyaA* mutant. WT MG1655 and Δ*cyaA* cells were grown at 37°C to the mid-log phase in LB prior to analyses. (**A**) Gene Ontology analysis of significantly downregulated pathways in Δ*cyaA* from RNA sequencing data. (**B**) Volcano plot of RNA sequencing results comparing Δ*cyaA* with WT. Marked genes involved in Thr and Trp catabolism were most significantly downregulated. (**C**) Fold change of selected genes comparing Δ*cyaA* with WT. (**D**) Concentrations of amino acids and ATP. *P* values were calculated using the unpaired *t*-test comparing the Δ*cyaA* mutant with the WT. * $P \leq 0.05$, ** $P \leq 0.01$. FDR, false discovery rate; FC, fold change.

tribution of cAMP is calculated as:

$$CV^2_{cAMP}/CV^2 = \left(CV^2 - CV^2_{other}\right)/CV^2$$

CV^2 is the noise in P*rrsC* activity or UGA readthrough in WT as computed above, and $CV_{other}{}^2$ is the noise in the absence of cAMP in the Δ*cyaA* strain.

Statistical analyses

Experiments were performed using at least three biological replicates. Individual dots represent distinct samples. In all cases, error bars represent the standard deviations (SD). All statistical analysis was performed in SPSSStatistics (v 25.0) or Prism (v 9.5.0). Statistical differences were analyzed using the unpaired t-test. Differences were considered significant at a *P* value <0.05.

RESULTS

High-throughput screening for *E. coli* mutants with altered UGA readthrough

Increasing evidence shows that translational fidelity is regulated by genetic and environmental cues, and plays crucial roles in fitness and adaptation. We have previously constructed dual-fluorescence reporters to detect stop-codon readthrough in bacterial populations and single cells (14). These reporters allow convenient and high-throughput quantitation of translational errors. To search for novel genes that are important for translational fidelity, we introduced the UGA readthrough reporter (pZS-P*tet*-m-TGA-y) and the control (pZS-P*tet*-m-y) plasmids into the Keio knockout collection (44) in 96-well plates (Figure 1). The transformants were then cultured in fresh Luria Broth (LB)

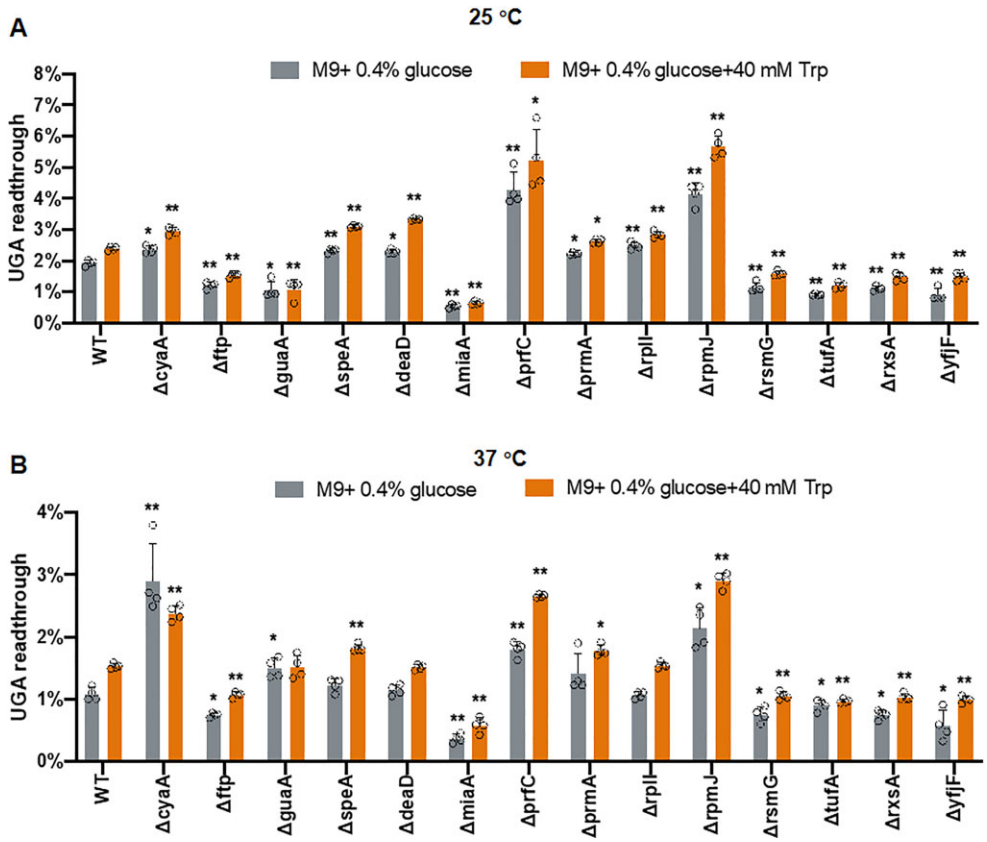

Figure 5. UGA readthrough of *E. coli* variants in minimal media. Overnight cultures of *E. coli* with pZS-P*tet*-m-TGA-y and pZS-P*tet*-m-y were diluted 1:50 in M9 media and incubated at (**A**) 25°C or (**B**) 37°C for 16 h. The UGA readthrough levels were determined as in Figure 1. Error bars indicate standard deviations. *P* values were calculated using the unpaired *t*-test comparing the mutants with the WT. * $P \leq 0.05$, ** $P \leq 0.01$.

over 16 h at 25 and 37°C, respectively. The mCherry and YFP signals were quantitated with a platereader, and the UGA readthrough levels were determined using the ratio of YFP over mCherry as described (14).

A total of ∼4000 strains covering the entire Keio collection were screened. Growing the wild-type strain BW25113 at 25 and 37°C yielded ∼4% and 2% of UGA readthrough, respectively (Figure 1C, D). Using the cutoff of either a 1.5-fold increase or decrease in the UGA readthrough level at 25°C, we identified a total of 30 knockout strains as potential hits. Based on the functions, we grouped the 30 genes into metabolism, translation, transcription, redox and other (Figure 1 and Table S1). Among the identified genes from our screening, *miaA*, *prfC*, *rplI* and *rsmG* are translational factors that have previously been associated with translational fidelity. MiaA catalyzes the isopentenyladenosine modification at position 37 (i^6A37) of tRNAs, and its deletion decreases UGA readthrough (45); it also plays an important role in the general stress response (46). The *prfC* gene encodes RF3, which facilitates RF1 and RF2 to terminate translation at stop codons (47). *rplI* encodes the L9 protein of the ribosome and deleting *rplI* increases translational readthrough, frameshift and recoding of stalled ribosomes (48,49). RsmG (GidB) is a ribosomal RNA (rRNA) methyltransferase and has been shown to increase some types of amino acid misincorporation in *Mycobacteria tuberculosis* (50). Among the newly identified genetic factors that affect stop-codon readthrough, *tufA* is one of the two genes that encode elongation factor Tu (EF-Tu). During translation termination, EF-Tu forms a ternary complex (TC) with aa-tRNA and GTP to compete with release factors and suppress stop codons (Figure 1A). A reduction in TC in the Δ*tufA* strain would explain a decrease in UGA readthrough. Many of the remaining genes are involved in cellular metabolism. For instance, CyaA is the only enzyme in *E. coli* to catalyze the synthesis of cAMP, which regulates the expression of metabolic pathways when bound to CRP (51,52); GuaA is one of the two enzymes in *E. coli* that synthesizes GMP (53); SpeA contributes to the biosynthesis of polyamines (54).

To validate the roles of the identified genes in UGA readthrough, we performed complementation experiments by introducing overexpression plasmids into the corresponding knockout strains (55). UGA readthrough of most deletion strains was largely restored to the wild-type (WT) level, except for Δ*prmA*, Δ*rho*, Δ*fkpB*, Δ*proW*, Δ*yaiY* and Δ*yfjF* (Figure S1). The lack of complementation could result from secondary mutations in the Keio knockout strains, dosage effects of gene expression, polar effects on the expression of neighboring genes, or nonfunctional proteins due to the N-terminal histidine tag on the ASKA plasmids.

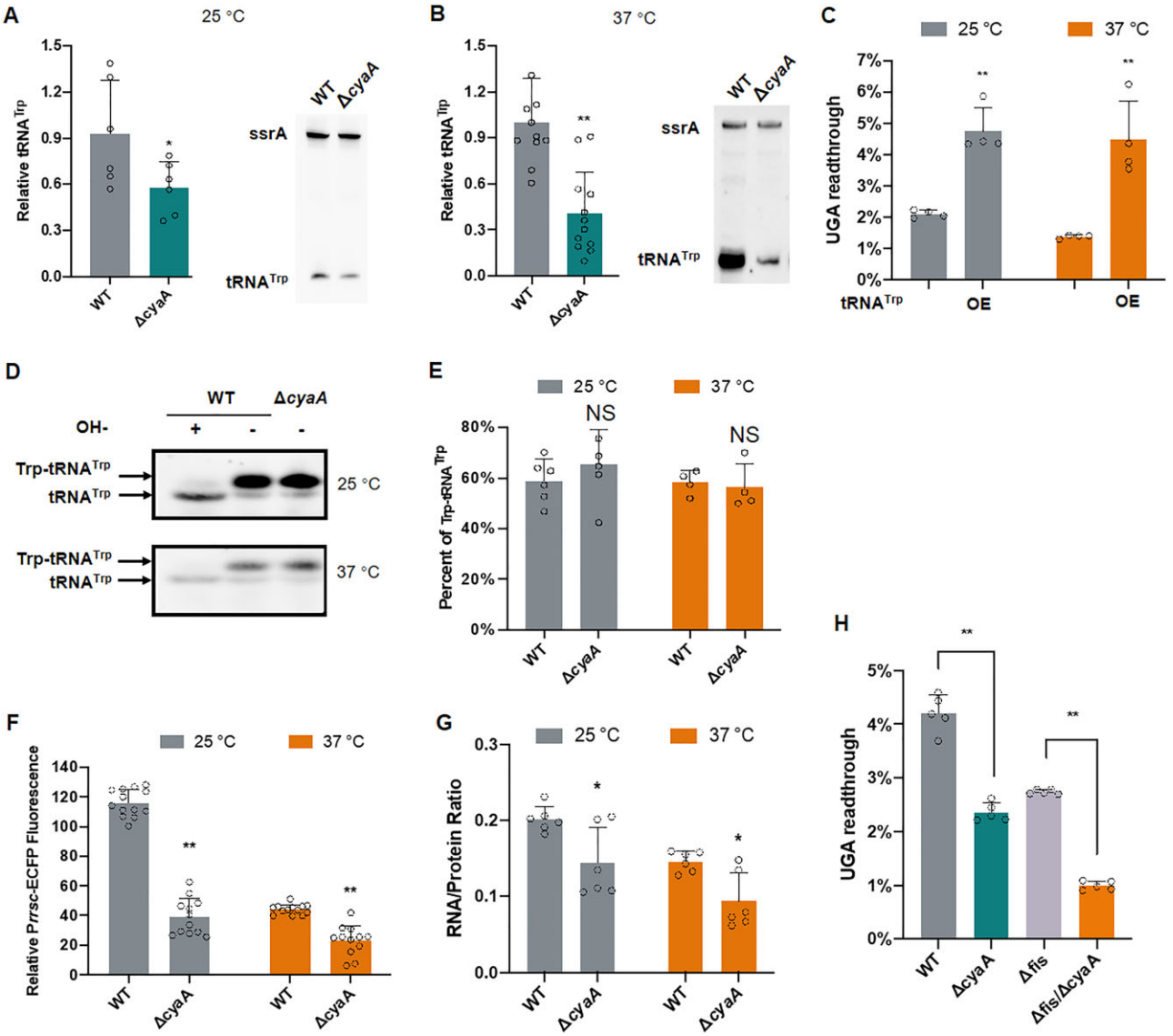

Figure 6. CyaA regulates the biogenesis of rRNAs and $tRNA^{Trp}$. (**A, B**) The levels of $tRNA^{Trp}$ were shown by northern blot. MG1655-derived cells were grown at 25°C or 37°C to the mid-log phase in LB. (**C**) Overexpressing (OE) $tRNA^{Trp}$ on a plasmid increased UGA readthrough in the Δ*cyaA* mutant. (**D**) Acidic gel northern blot against $tRNA^{Trp}$. Alkaline (OH–) treatment deacylated Trp-$tRNA^{Trp}$ to form $tRNA^{Trp}$. Most of $tRNA^{Trp}$ in both WT and Δ*cyaA* were charged with Trp. (**E**) Quantitation of the results in (D). The percentage was calculated by dividing the level of Trp-$tRNA^{Trp}$ by Trp-$tRNA^{Trp}$ + $tRNA^{Trp}$. (**F**) Promoter activities of *rrsC*. Overnight cultures harboring pZS-P*tet*-m-TGA-y-P*rrsC*-eCFP were diluted 1:50 in fresh LB Amp and incubated at 25°C or 37°C for 16 h. The promoter activity was calculated as the ratio of eCFP over mCherry. (**G**) RNA/protein ratio. (**H**) UGA readthrough was determined using pZS-P*tet*-m-TGA-y at 25°C as in Figure 1. The Error bars indicate standard deviations. P values were calculated using the unpaired *t*-test comparing the mutants with the WT. * $P \leq 0.05$, ** $P \leq 0.01$.

Translational fidelity of knockout mutants derived from MG1655

To rule out the effects of nonspecific mutations in the Keio strains on UGA readthrough, we constructed 18 deletion mutants from *E. coli* MG1655 (Tables S2 and S3). The 12 other genes were left out due to the redundant pathways (*crp* and *rsxBCDEF*), no effect on UGA readthrough at 37°C (*purA* and *hns*), or difficulty in deletion (*ubiEFH* and *rho*). The UGA readthrough levels of MG1655-derived mutants all confirmed the changes seen in the Keio strains except for Δ*rimP*, Δ*proW* and Δ*yaiY*, which showed no significant change in UGA readthrough at 25°C (Figure 2A, B).

We next tested how the deletion of these genes affects other types of translational errors. Due to the low frequencies of UAG readthrough and misincorporation, we used dual-luciferase reporters as previously described (10,13). Deleting *cyaA*, *guaA*, *miaA*, *tufA* and *yfjF* decreased both UAG and UGA readthrough but had no effect on lysine misincorporation at AAU asparagine codons (Figure 2D, E). This suggests that these genes specifically influence stop-codon readthrough. On the other hand, deleting *prfC*, *rplI*, *rpmJ* or *rsmG* affected both stop-codon readthrough and amino acid misincorporation, indicating their broader roles in the regulation of translational fidelity.

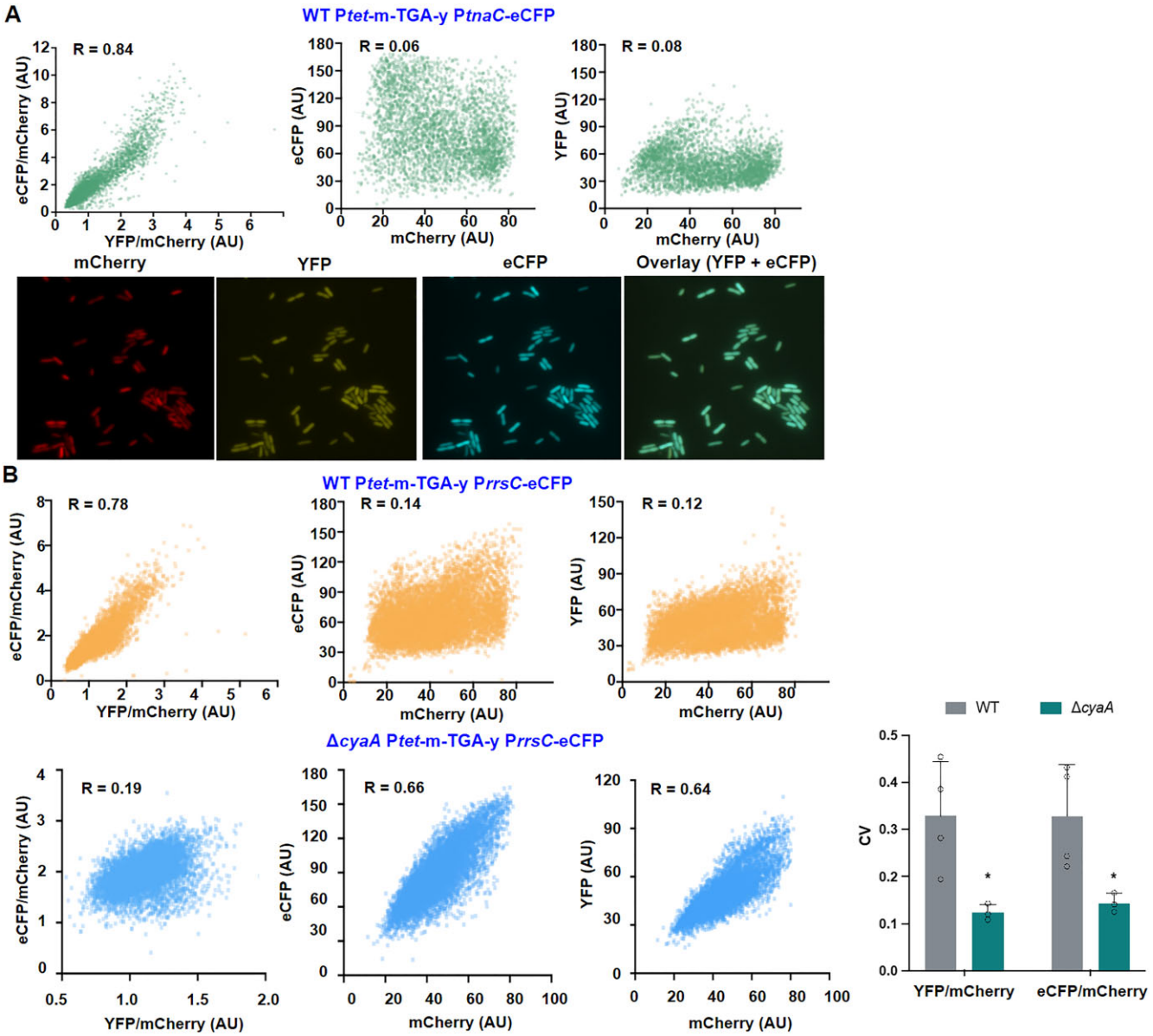

Figure 7. Cyclic AMP drives heterogeneity of UGA readthrough in single cells. MG1655-derived *E. coli* cells carrying pZS-P*tet*-m-TGA-y P*tnaC*-eCFP or pZS-P*tet*-m-TGA-y P*rrsC*-eCFP were grown at 37°C for 24 hours prior to fluorescence imaging. Over 3000 cells were analyzed for each sample. (**A**) WT MG1655 cells carrying pZS-P*tet*-m-TGA-y P*tnaC*-eCFP. The signal of cAMP reporter P*tnaC*-eCFP strongly correlates with the relative UGA readthrough level indicated by YFP/mCherry. (**B**) The *rrsC* promoter activity is strongly correlated with UGA readthrough in the WT, but not in the Δ*cyaA* mutant. AU, arbitrary unit; R, correlation coefficient. CV, coefficient of variation, calculated as the ration of standard deviation and mean. The CV of YFP/mCherry indicates the heterogeneity of UGA readthrough and the CV of eCFP/mCherry indicates the heterogeneity of P*rrsC* activity.

To further test how the identified genes affect the readthrough of native stop codons, we used a published NudL construct with an N-terminal FLAG tag and a streptavidin tag after the stop codon (56). Readthrough of the native UGA stop codon of *nudL* yielded an extended protein (Figure 2F). For all the tested mutants, the changes in the efficiency of UGA readthrough in the *nudL* gene were consistent with the reporter assay (Figures 2C, F, G).

The growth rate of WT MG1655 was twice at 37°C as compared to 25°C (Figure S2A), yet the UGA readthrough rate was about 50% lower at 37°C than that at 25°C (Figure 1). To test if growth rates are broadly associated with the UGA readthrough levels, we performed growth assays of MG1655-derived mutants and did not observe an apparent correlation between the two (Figure S2).

Single-cell analyses of UGA readthrough in *E. coli* variants

Our dual-fluorescence reporter (m-TGA-y) not only empowers us to perform high-throughput screening but also allows us to observe UGA readthrough in single cells (14,16). We detected YFP signals resulting from readthrough in WT cells using both fluorescence microscopy (Figures S3, S4) and flow cytometry (Figure S5). Overall, UGA readthrough was heterogeneous among sin-

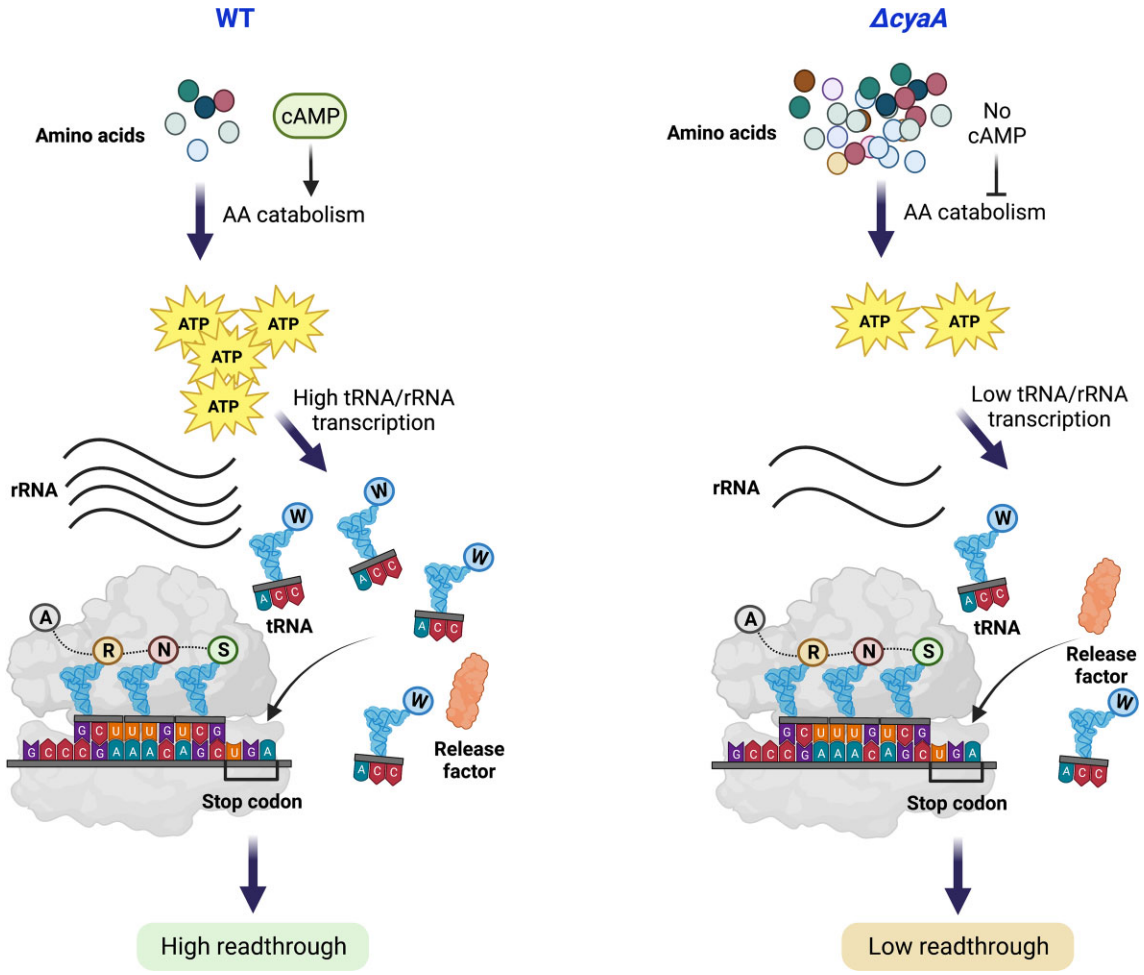

Figure 8. Model for regulation of UGA readthrough by cAMP. The cAMP level fluctuates stochastically among individual cells. A high cAMP level activates the expression of catabolic genes, which leads to the efficient utilization of amino acids as a carbon source and robust ATP synthesis. A high ATP level promotes transcription of rRNAs and tRNAs, resulting in more Trp-tRNA^{Trp} to effectively compete with release factor 2 and increase UGA readthrough. Created with BioRender.com.

gle cells in the same population, and the single-cell results agreed well with the population-based platereader results (Figures 2, S4, S5). Both Δ*cyaA* and Δ*guaA* cells show brighter mCherry signals compared with the WT (Figure S4), presumably due to slow growth (Figure S2) that results in the accumulation of stable fluorescent proteins. Despite the high mCherry levels, the YFP signals in the Δ*cyaA* and Δ*guaA* cells were weaker than in the WT (Figure S4), indicating lower UGA readthrough levels in these mutant cells.

Impact of release factors on UGA readthrough

The UGA readthrough level is primarily determined by the competition between the EF-Tu:Trp-tRNA^{Trp}:GTP ternary complex and RF2, which is facilitated by GTP-bound RF3 (14,47). Overexpressing RF2 did not substantially decrease UGA readthrough in most of the tested variants (Figure 3A). Overexpressing both RF2 and RF3 decreased UGA readthrough in most variant strains (Figure 3B), supporting the coordinated function of RF2 and RF3 in releasing the ribosome from UGA codons.

We next deleted RF3 in the WT and single knockout mutants. Further deletion of RF3 increased UGA readthrough in all the tested variants (Figure 3C). Interestingly, deleting RF3 in Δ*guaA* and WT abolished the difference in UGA readthrough between the two strains, implying that GuaA primarily affects UGA readthrough via RF3. As GuaA facilitates the biosynthesis of GMP and GTP, it likely enhances stop-codon readthrough by increasing the level of GTP-bound RF3.

Cyclic AMP regulates amino acid and ATP metabolism

Our initial screening shows that deleting either *cyaA* or *crp* decreases stop-codon readthrough (Figure 1), implying a previously unknown role of cAMP-CRP in translational regulation. Supplementing cAMP in the medium indeed restored UGA readthrough in the Δ*cyaA* mutant (Figure S6A). Cyclic AMP has been considered a central regulator of carbon metabolism (52). In line with this, our RNA sequencing results show that deleting *cyaA* causes significant downregulation of genes involved in amino acid catabolism and ATP biosynthesis in *E. coli* cells grown in LB (Figures

4A–C, Table S2). LB medium uses oligopeptides and amino acids as the main carbon source (57). Downregulation of amino acid catabolic genes is expected to cause amino acid accumulation and lower energy production. Indeed, quantitative metabolomics revealed that the total amino acid concentration in the Δ*cyaA* mutant was 2-fold higher compared with that in the WT (Figure 4D, Table S3). In particular, tryptophan and threonine concentrations were increased over 10-fold upon deletion of *cyaA*, consistent with Trp and Thr catabolic genes being among the top downregulated genes in the Δ*cyaA* mutant (Figure 4). We next determined the cellular ATP levels using a previously developed luciferase assay (58). Deleting *cyaA* decreased the ATP level by ∼50% (Figure 4D), supporting that cAMP maintains efficient amino acid catabolism and ATP production in *E. coli* grown in LB.

To further test the role of amino acid catabolism in cAMP-regulated stop-codon readthrough, we grew *E. coli* variants in minimal media (M9) with glucose as the carbon source. Opposite to LB with peptides as the carbon source (Figure 2), deleting *cyaA* caused higher UGA readthrough than the WT in M9 glucose (Figure 5). In comparison, other deletion mutants mostly exhibited similar effects on UGA readthrough in M9 and LB. These results support that regulation of stop-codon readthrough by cAMP depends on carbon metabolism.

Cyclic AMP enhances the biogenesis of rRNAs and tRNA^{Trp}

The TC/RF competition model for UGA readthrough indicates that the levels of Trp-tRNA^{Trp}, EF-Tu or RF2 may affect UGA readthrough (14). Western blot results revealed that the concentrations of EF-Tu and RF2 were not significantly affected upon deletion of *cyaA* (Figure S7). In contrast, the level of total tRNA^{Trp} decreased in Δ*cyaA* at both 25 and 37°C (Figures 6A, B). Overexpressing tRNA^{Trp} also increased UGA readthrough in the Δ*cyaA* background (Figure 6C). We next measured the aminoacylation percentage of tRNA^{Trp} using acidic-gel northern blot. Deleting *cyaA* did not affect the percentage of Trp-tRNA^{Trp} despite an increase in the Trp concentration (Figures 4D, 6D, E). Given the decrease of total tRNA^{Trp} in the Δ*cyaA* mutant, we estimated that the Trp-tRNA^{Trp} level decreased by approximately 50% upon deletion of *cyaA*.

In bacteria, many tRNAs are transcribed in the same operon as rRNAs. For instance, the gene encoding tRNA^{Trp} is within the *rrsC* rRNA operon in *E. coli*. It has been previously shown that increasing the ATP level enhances the promoter activity of *rrn* P1 (including *rrsC*), which contains an A in the transcription initiation site (59). Given the decrease of ATP in the Δ*cyaA* mutant, we hypothesized that cAMP may positively regulate rRNA and tRNA transcription. To test this, we constructed an eCFP reporter under the control of the *rrsC* promoter, normalized by the mCherry signal under the control of the constitutive *tet* promoter. Deleting *cyaA* indeed significantly decreased the *rrsC* promoter activity (Figure 6F). The rRNA content has been previously measured using the RNA/protein ratio (60). We found that the RNA/protein ratio was lower in the Δ*cyaA* mutant, indicating impaired rRNA biogenesis (Figure 6G). Ribosome inhibitors such as chloramphenicol (Chl) increase the RNA/protein ratio and the tRNA^{Trp} level (14,60). In the presence of Chl, the tRNA^{Trp} and UGA readthrough levels substantially increased in both the WT and Δ*cyaA* mutant (Figure S8). Previous work also identified Fis as a positive regulator of rRNA transcription (61). Deleting *cyaA* in the Δ*fis* background still resulted in a decrease in UGA readthrough (Figure 6H), suggesting that the role of cAMP in rRNA and tRNA transcription does not depend on Fis. Collectively, our data suggest that cAMP enhances the transcription of rRNAs and tRNA^{Trp} by increasing the concentration of ATP.

Cyclic AMP drives heterogeneity of UGA readthrough in single cells

Our previous work shows that UGA readthrough is heterogeneous among single cells (14). However, the source of such heterogeneity has not been identified. To test the role of cAMP in UGA readthrough at the single-cell level, we constructed a triple-fluorescence reporter with P*tet*-mCherry-UGA-YFP P*tnaC*-eCFP. We confirmed that P*tnaC* activity depended on cAMP as deleting *cyaA* abolished eCFP fluorescence, which was restored by supplementation of cAMP in the medium (Figure S6B). Among single cells, the expression level of P*tnaC*-eCFP strongly correlated with the UGA readthrough level (Figure 7A). In addition, the P*rrsC* activity also strongly correlated with UGA readthrough in the WT, but not in the Δ*cyaA* strain (Figure 7B). Given that deleting *cyaA* causes a decrease in UGA readthrough (Figures 2, S4, S5), these data suggest that fluctuation of the cAMP level among single cells leads to altered tRNA^{Trp} expression and promotes the heterogeneity of UGA readthrough. In line with this, deleting *cyaA* enhanced the correlation between YFP and mCherry of the m-TGA-y reporter, with an increase of the R-value from 0.12 to 0.64 (Figure 7B), indicating decreased heterogeneity of UGA readthrough upon depletion of cAMP. Heterogeneity of gene expression is typically quantified using coefficient of variation (CV) (43,62,63). Deleting *cyaA* significantly decreased the CV of both UGA readthrough and P*rrsC* activity (Figure 7B). Further analysis of noise decomposition shows that fluctuation in cAMP contributes to ∼85% of noise in UGA readthrough and P*rrsC* expression (see Materials and Methods).

DISCUSSION

Early studies of streptomycin-resistant *E. coli* mutants have led to the discovery of the critical roles that ribosomal genes *rpsD* (uS4) and *rpsL* (uS12) play in maintaining translational fidelity (64,65). Random mutagenesis of *rpsL* and rRNA genes has later been performed to identify mutations that affect ribosomal fidelity (25,66,67). More recently, suppression of stop codons has attracted tremendous interest in the treatment of genetic diseases caused by nonsense mutations (68–73). Several studies have used luminescence-based assays to screen for small compounds that promote the readthrough of stop codons (73,74). In this work, we have used an economical and convenient dual-fluorescence reporter assay to perform systematic and

genome-wide screening for genes that affect translational fidelity. Compared with transposon-based selection, screening of a defined knockout library allows us to identify genes that either increase or decrease translational errors. Our screening has revealed a total of 30 nonessential genes in *E. coli* that affect stop-codon readthrough and most of them have not been previously shown to regulate translational fidelity.

In addition to revealing genetic networks critical for maintaining translational fidelity, our work here also provides a useful resource for future studies of synthetic biology and genetic code expansion. Assigning stop codons to noncanonical amino acids has been developed as a powerful tool to engineer proteins and expand the genetic code in synthetic organisms (75–77). A significant challenge is the suppression of stop codons by endogenous amino acids in recoded organisms. It would be interesting to explore the genes identified in this study to decrease readthrough of stop codons by endogenous amino acids and enhance the translation efficiency of noncanonical amino acids.

Growing evidence suggests that translational fidelity is associated with cellular metabolism. Competition between tRNAs affects the rates of amino acid misincorporation (10,78), and fluctuations in amino acid concentrations are predicted to affect the fidelity of aa-tRNA synthesis (5). Stop-codon readthrough is affected by pH (16,79,80). In this work, we have uncovered a previously unknown central role of cAMP in coupling carbon metabolism with the regulation of translational fidelity. It is well-established that cAMP-CRP regulates carbon metabolism (52). Cyclic AMP also plays important roles in microbial pathogenesis through the regulation of biofilm formation, Type III secretion and other virulence genes in various pathogens(81). Additionally, it has been shown that cAMP coordinates the allocation of the proteome (42). Our RNA sequencing and metabolomics data demonstrate that deleting *cyaA*, the sole adenylate cyclase in *E. coli*, leads to significant downregulation of amino acid catabolic genes and accumulation of amino acids in cells grown in LB (Figure 4). This results in a decrease in the ATP level, lowering transcription of rRNAs and tRNAs including $tRNA^{Trp}$ (Figures 4, 6, 7). Although deleting *cyaA* increases the cellular level of Trp (Figure 4D), it does not significantly increase the aminoacylation level of $tRNA^{Trp}$ (Figure 6D). Therefore, the overall Trp-$tRNA^{Trp}$:EF-Tu:GTP ternary complex is decreased in the Δ*cyaA* mutant, leading to a lower level of UGA readthrough (Figure 8). A recent study shows that in rich media with abundant amino acids, *E. coli* expresses a high level of the protein synthesis machinery (82). Our work here has uncovered a previously unknown role of cAMP in controlling the biogenesis of rRNAs and tRNAs in rich media.

Gene expression is intrinsically noisy and such noise may lead to phenotypic heterogeneity that benefits the microbial population during environmental changes (43,83,84). We and others have previously shown that translational fidelity in heterogeneous in bacterial and mammalian cells (14,36,85,86). However, little is known about the sources driving the heterogeneity of translational errors. Our work here suggests that cAMP is a key driver of heterogeneity in both UGA readthrough and rRNA expression among single *E. coli* cells (Figure 7). Single cells with higher UGA readthrough appear to grow better in minimal media but are more sensitive to stress (14,16). Future work is warranted to elucidate how altering translational fidelity affects cellular metabolism and fitness at both the single-cell and population levels.

DATA AVAILABILITY

The RNA sequencing data are deposited in Gene Expression Omnibus: https://www.ncbi.nlm.nih.gov/geo/query/acc.cgi?acc=GSE228051. Other data that support the findings of this study can be made available from the corresponding author upon reasonable request.

ACCESSION NUMBERS

The RNA sequencing data are deposited in Gene Expression Omnibus with the accession number GSE228051: https://www.ncbi.nlm.nih.gov/geo/query/acc.cgi?acc=GSE228051.

SUPPLEMENTARY DATA

Supplementary Data are available at NAR Online.

ACKNOWLEDGEMENTS

We would like to thank Dr Philip J. Farabaugh (University of Maryland) for providing the dual-luciferase constructs pEK 4 and pEK7, and Dr Carol Gross (University of California San Francisco) for providing the NudL construct.
Author contributions: Z.L., P.V., L.O., P.M. and J.L. designed and performed the experiments. Z.L., P.V., L.O., P.M., J.A., V.B., A.S. and J.L. analyzed the data. Z.L. and J.L. wrote the manuscript. All authors proofread the manuscript.

FUNDING

National Institute of General Medical Sciences [R35GM136213 to J.L.]. Funding for open access charge: National Institute of General Medical Sciences [R35GM136213].
Conflict of interest statement. None declared.

REFERENCES

1. Zaher,H.S. and Green,R. (2009) Fidelity at the molecular level: lessons from protein synthesis. *Cell*, **136**, 746–762.
2. Ling,J., Reynolds,N. and Ibba,M. (2009) Aminoacyl-tRNA synthesis and translational quality control. *Annu. Rev. Microbiol.*, **63**, 61–78.
3. Rozov,A., Demeshkina,N., Westhof,E., Yusupov,M. and Yusupova,G. (2015) Structural insights into the translational infidelity mechanism. *Nat. Commun.*, **6**, 7251.
4. Ling,J., O'Donoghue,P. and Söll,D. (2015) Genetic code flexibility in microorganisms: novel mechanisms and impact on physiology. *Nat. Rev. Micro.*, **13**, 707–721.
5. Rubio Gomez,M.A. and Ibba,M. (2020) Aminoacyl-tRNA synthetases. *RNA*, **26**, 910–936.
6. Nagy,K., A.B.,B. and Musier-Forsyth,K. (2020) Trans-editing by aminoacyl-tRNA synthetase-like editing domains. *Enzymes*, **48**, 69–115.
7. Martinis,S.A. and Boniecki,M.T. (2010) The balance between pre- and post-transfer editing in tRNA synthetases. *FEBS Lett.*, **584**, 455–459.

8. Rodnina,M.V. and Wintermeyer,W. (2001) Ribosome fidelity: TRNA discrimination, proofreading and induced fit. *Trends Biochem. Sci.*, **26**, 124–130.
9. Bradley,C.C., Gordon,A.J.E., Halliday,J.A. and Herman,C. (2019) Transcription fidelity: new paradigms in epigenetic inheritance, genome instability and disease. *DNA Repair (Amst.)*, **81**, 102652.
10. Kramer,E.B. and Farabaugh,P.J. (2007) The frequency of translational misreading errors in *E. coli* is largely determined by tRNA competition. *RNA*, **13**, 87–96.
11. Mohler,K., Aerni,H.R., Gassaway,B., Ling,J., Ibba,M. and Rinehart,J. (2017) MS-READ: quantitative measurement of amino acid incorporation. *Biochim. Biophys. Acta*, **1861**, 3081–3088.
12. Mordret,E., Dahan,O., Asraf,O., Rak,R., Yehonadav,A., Barnabas,G.D., Cox,J., Geiger,T., Lindner,A.B. and Pilpel,Y. (2019) Systematic detection of amino acid substitutions in proteomes reveals mechanistic basis of ribosome errors and selection for translation fidelity. *Mol. Cell*, **75**, 427–441.
13. Devaraj,A., Shoji,S., Holbrook,E.D. and Fredrick,K. (2009) A role for the 30S subunit E site in maintenance of the translational reading frame. *RNA*, **15**, 255–265.
14. Fan,Y., Evans,C.R., Barber,K.W., Banerjee,K., Weiss,K.J., Margolin,W., Igoshin,O.A., Rinehart,J. and Ling,J. (2017) Heterogeneity of stop codon readthrough in single bacterial cells and implications for population fitness. *Mol. Cell*, **67**, 826–836.
15. Engelberg-Kulka,H. (1981) UGA suppression by normal $tRNA^{Trp}$ in *Escherichia coli*: codon context effects. *Nucleic Acids Res.*, **9**, 983–991.
16. Zhang,H., Lyu,Z., Fan,Y., Evans,C.R., Barber,K.W., Banerjee,K., Igoshin,O.A., Rinehart,J. and Ling,J. (2020) Metabolic stress promotes stop-codon readthrough and phenotypic heterogeneity. *P. Natl. Acad. Sci. U.S.A.*, **117**, 22167–22172.
17. Schwartz,M.H., Waldbauer,J.R., Zhang,L. and Pan,T. (2016) Global tRNA misacylation induced by anaerobiosis and antibiotic exposure broadly increases stress resistance in *Escherichia coli*. *Nucleic Acids Res.*, **44**, 10292–10303.
18. Steiner,R.E., Kyle,A.M. and Ibba,M. (2019) Oxidation of phenylalanyl-tRNA synthetase positively regulates translational quality control. *Proc. Natl. Acad. Sci. U.S.A.*, **116**, 10058–10063.
19. Lant,J.T., Kiri,R., Duennwald,M.L. and O'Donoghue,P. (2021) Formation and persistence of polyglutamine aggregates in mistranslating cells. *Nucleic Acids Res.*, **49**, 11883–11899.
20. Schmidt,E. and Schimmel,P. (1994) Mutational isolation of a sieve for editing in a transfer RNA synthetase. *Science*, **264**, 265–267.
21. Roy,H., Ling,J., Irnov,M. and Ibba,M. (2004) Post-transfer editing *in vitro* and *in vivo* by the beta subunit of phenylalanyl-tRNA synthetase. *EMBO J.*, **23**, 4639–4648.
22. Beuning,P.J. and Musier-Forsyth,K. (2000) Hydrolytic editing by a class II aminoacyl-tRNA synthetase. *Proc. Natl. Acad. Sci. U.S.A.*, **97**, 8916–8920.
23. Dock-Bregeon,A., Sankaranarayanan,R., Romby,P., Caillet,J., Springer,M., Rees,B., Francklyn,C.S., Ehresmann,C. and Moras,D. (2000) Transfer RNA-mediated editing in threonyl-tRNA synthetase. The class II solution to the double discrimination problem. *Cell*, **103**, 877–884.
24. Lant,J.T., Berg,M.D., Heinemann,I.U., Brandl,C.J. and O'Donoghue,P. (2019) Pathways to disease from natural variations in human cytoplasmic tRNAs. *J. Biol. Chem.*, **294**, 5294–5308.
25. McClory,S.P., Leisring,J.M., Qin,D. and Fredrick,K. (2010) Missense suppressor mutations in 16S rRNA reveal the importance of helices h8 and h14 in aminoacyl-tRNA selection. *RNA*, **16**, 1925–1934.
26. Zimmermann,R.A., Garvin,R.T. and Gorini,L. (1971) Alteration of a 30S ribosomal protein accompanying the ram mutation in *Escherichia coli*. *Proc. Natl. Acad. Sci. U.S.A.*, **68**, 2263–2267.
27. Dinman,J.D. (2019) Translational recoding signals: expanding the synthetic biology toolbox. *J. Biol. Chem.*, **294**, 7537–7545.
28. Choi,J., O'Loughlin,S., Atkins,J.F. and Puglisi,J.D. (2020) The energy landscape of -1 ribosomal frameshifting. *Sci. Adv.*, **6**, eaax6969.
29. Ling,J. and Söll,D. (2010) Severe oxidative stress induces protein mistranslation through impairment of an aminoacyl-tRNA synthetase editing site. *Proc. Natl. Acad. Sci. U.S.A.*, **107**, 4028–4033.
30. Mohler,K. and Ibba,M. (2017) Translational fidelity and mistranslation in the cellular response to stress. *Nat. Microbiol.*, **2**, 17117.
31. Martinez-Miguel,V.E., Lujan,C., Espie-Caullet,T., Martinez-Martinez,D., Moore,S., Backes,C., Gonzalez,S., Galimov,E.R., Brown,A.E.X., Halic,M. *et al.* (2021) Increased fidelity of protein synthesis extends lifespan. *Cell Metab.*, **33**, 2288–2300.
32. Shcherbakov,D., Nigri,M., Akbergenov,R., Brilkova,M., Mantovani,M., Petit,P.I., Grimm,A., Karol,A.A., Teo,Y., Sanchon,A.C. *et al.* (2022) Premature aging in mice with error-prone protein synthesis. *Sci. Adv.*, **8**, eabl9051.
33. Lyu,Z., Wilson,C. and Ling,J. (2023) Translational fidelity during bacterial stresses and host interactions. *Pathogens*, **12**, 383.
34. Fan,Y., Wu,J., Ung,M.H., De Lay,N., Cheng,C. and Ling,J. (2015) Protein mistranslation protects bacteria against oxidative stress. *Nucleic Acids Res.*, **43**, 1740–1748.
35. Fan,Y., Thompson,L., Lyu,Z., Cameron,T.A., De Lay,N.R., Krachler,A.M. and Ling,J. (2019) Optimal translational fidelity is critical for *Salmonella* virulence and host interactions. *Nucleic Acids Res.*, **47**, 5356–5367.
36. Su,H.W., Zhu,J.H., Li,H., Cai,R.J., Ealand,C., Wang,X., Chen,Y.X., Kayani,M.U., Zhu,T.F., Moradigaravand,D. *et al.* (2016) The essential mycobacterial amidotransferase GatCAB is a modulator of specific translational fidelity. *Nat. Microbiol.*, **1**, 16147.
37. Javid,B., Sorrentino,F., Toosky,M., Zheng,W., Pinkham,J.T., Jain,N., Pan,M., Deighan,P. and Rubin,E.J. (2014) Mycobacterial mistranslation is necessary and sufficient for rifampicin phenotypic resistance. *Proc. Natl. Acad. Sci. U.S.A.*, **111**, 1132–1137.
38. Datsenko,K.A. and Wanner,B.L. (2000) One-step inactivation of chromosomal genes in *Escherichia coli* K-12 using PCR products. *Proc. Natl. Acad. Sci. U.S.A.*, **97**, 6640–6645.
39. Dang,D., Le,M., Irmer,T., Angay,O., Fichtl,B. and Schwarz,B. (2021) APEER: an interactive cloud platform for microscopists to easily deploy deep learning. *Zenodo*, https://doi.org/10.5281/zenodo.5539895.
40. Pachitariu,M. and Stringer,C. (2022) Cellpose 2.0: how to train your own model. *Nat. Methods*, **19**, 1634–1641.
41. Stringer,C., Wang,T., Michaelos,M. and Pachitariu,M. (2021) Cellpose: a generalist algorithm for cellular segmentation. *Nat. Methods*, **18**, 100–106.
42. You,C., Okano,H., Hui,S., Zhang,Z., Kim,M., Gunderson,C.W., Wang,Y.P., Lenz,P., Yan,D. and Hwa,T. (2013) Coordination of bacterial proteome with metabolism by cyclic AMP signalling. *Nature*, **500**, 301–306.
43. Elowitz,M.B., Levine,A.J., Siggia,E.D. and Swain,P.S. (2002) Stochastic gene expression in a single cell. *Science*, **297**, 1183–1186.
44. Baba,T., Ara,T., Hasegawa,M., Takai,Y., Okumura,Y., Baba,M., Datsenko,K.A., Tomita,M., Wanner,B.L. and Mori,H. (2006) Construction of *Escherichia coli* K-12 in-frame, single-gene knockout mutants: the Keio collection. *Mol. Syst. Biol.*, **2**, 2006.0008.
45. Petrullo,L.A., Gallagher,P.J. and Elseviers,D. (1983) The role of 2-methylthio-N6-isopentenyladenosine in readthrough and suppression of nonsense codons in *Escherichia coli*. *Mol. Gen. Genet.*, **190**, 289–294.
46. Thompson,K.M. and Gottesman,S. (2014) The MiaA tRNA modification enzyme is necessary for robust RpoS expression in *Escherichia coli*. *J. Bacteriol.*, **196**, 754–761.
47. Youngman,E.M., McDonald,M.E. and Green,R. (2008) Peptide release on the ribosome: mechanism and implications for translational control. *Annu. Rev. Microbiol.*, **62**, 353–373.
48. Herr,A.J., Nelson,C.C., Wills,N.M., Gesteland,R.F. and Atkins,J.F. (2001) Analysis of the roles of tRNA structure, ribosomal protein L9, and the bacteriophage T4 gene 60 bypassing signals during ribosome slippage on mRNA. *J. Mol. Biol.*, **309**, 1029–1048.
49. Seidman,J.S., Janssen,B.D. and Hayes,C.S. (2011) Alternative fates of paused ribosomes during translation termination. *J. Biol. Chem.*, **286**, 31105–31112.
50. Wong,S.Y., Javid,B., Addepalli,B., Piszczek,G., Strader,M.B., Limbach,P.A. and Barry,C.E., 3rd. (2013) Functional role of methylation of G518 of the 16S rRNA 530 loop by GidB in *Mycobacterium tuberculosis*. *Antimicrob. Agents Chemother.*, **57**, 6311–6318.
51. Zheng,D., Constantinidou,C., Hobman,J.L. and Minchin,S.D. (2004) Identification of the CRP regulon using *in vitro* and *in vivo* transcriptional profiling. *Nucleic Acids Res.*, **32**, 5874–5893.
52. Chubukov,V., Gerosa,L., Kochanowski,K. and Sauer,U. (2014) Coordination of microbial metabolism. *Nat. Rev. Micro.*, **12**, 327–340.

53. Petersen,C. (1999) Inhibition of cellular growth by increased guanine nucleotide pools. Characterization of an *Escherichia coli* mutant with a guanosine kinase that is insensitive to feedback inhibition by GTP. *J. Biol. Chem.*, **274**, 5348–5356.
54. Maas,W.K. (1972) Mapping of genes involved in the synthesis of spermidine in *Escherichia coli*. *Mol. Gen. Genet.*, **119**, 1–9.
55. Kitagawa,M., Ara,T., Arifuzzaman,M., Ioka-Nakamichi,T., Inamoto,E., Toyonaga,H. and Mori,H. (2005) Complete set of ORF clones of *Escherichia coli* ASKA library (a complete set of *E. coli* K-12 ORF archive): unique resources for biological research. *DNA Res.*, **12**, 291–299.
56. Baggett,N.E., Zhang,Y. and Gross,C.A. (2017) Global analysis of translation termination in *E. coli*. *PLoS Genet.*, **13**, e1006676.
57. Sezonov,G., Joseleau-Petit,D. and D'Ari,R. (2007) Escherichia coli physiology in Luria-Bertani broth. *J. Bacteriol.*, **189**, 8746–8749.
58. Schneider,D.A. and Gourse,R.L. (2004) Relationship between growth rate and ATP concentration in *Escherichia coli*: a bioassay for available cellular ATP. *J. Biol. Chem.*, **279**, 8262–8268.
59. Murray,H.D., Schneider,D.A. and Gourse,R.L. (2003) Control of rRNA expression by small molecules is dynamic and nonredundant. *Mol. Cell*, **12**, 125–134.
60. Dai,X., Zhu,M., Warren,M., Balakrishnan,R., Patsalo,V., Okano,H., Williamson,J.R., Fredrick,K., Wang,Y.P. and Hwa,T. (2016) Reduction of translating ribosomes enables *Escherichia coli* to maintain elongation rates during slow growth. *Nat. Microbiol.*, **2**, 16231.
61. Hirvonen,C.A., Ross,W., Wozniak,C.E., Marasco,E., Anthony,J.R., Aiyar,S.E., Newburn,V.H. and Gourse,R.L. (2001) Contributions of UP elements and the transcription factor FIS to expression from the seven rrn P1 promoters in *Escherichia coli*. *J. Bacteriol.*, **183**, 6305–6314.
62. Blake,W.J., M,K.A., Cantor,C.R. and Collins,J.J. (2003) Noise in eukaryotic gene expression. *Nature*, **422**, 633–637.
63. Taniguchi,Y., Choi,P.J., Li,G.W., Chen,H., Babu,M., Hearn,J., Emili,A. and Xie,X.S. (2010) Quantifying *E. coli* proteome and transcriptome with single-molecule sensitivity in single cells. *Science*, **329**, 533–538.
64. Davies,J., Gilbert,W. and Gorini,L. (1964) Streptomycin, suppression, and the code. *Proc. Natl. Acad. Sci. U.S.A.*, **51**, 883–890.
65. Gorini,L. and Kataja,E. (1964) Phenotypic repair by streptomycin of defective genotypes in *E. coli*. *Proc. Natl. Acad. Sci. U.S.A.*, **51**, 487–493.
66. Agarwal,D., Gregory,S.T. and O'Connor,M. (2011) Error-prone and error-restrictive mutations affecting ribosomal protein S12. *J. Mol. Biol.*, **410**, 1–9.
67. Qin,D., Abdi,N.M. and Fredrick,K. (2007) Characterization of 16S rRNA mutations that decrease the fidelity of translation initiation. *RNA*, **13**, 2348–2355.
68. Ng,M.Y., Li,H., Ghelfi,M.D., Goldman,Y.E. and Cooperman,B.S. (2021) Ataluren and aminoglycosides stimulate read-through of nonsense codons by orthogonal mechanisms. *Proc. Natl. Acad. Sci. U.S.A.*, **118**, e2020599118.
69. Roy,B., Friesen,W.J., Tomizawa,Y., Leszyk,J.D., Zhuo,J., Johnson,B., Dakka,J., Trotta,C.R., Xue,X., Mutyam,V. *et al.* (2016) Ataluren stimulates ribosomal selection of near-cognate tRNAs to promote nonsense suppression. *Proc. Natl. Acad. Sci. U.S.A.*, **113**, 12508–12513.
70. Wang,J., Zhang,Y., Mendonca,C.A., Yukselen,O., Muneeruddin,K., Ren,L., Liang,J., Zhou,C., Xie,J., Li,J. *et al.* (2022) AAV-delivered suppressor tRNA overcomes a nonsense mutation in mice. *Nature*, **604**, 343–348.
71. Beznoskova,P., Bidou,L., Namy,O. and Valasek,L.S. (2021) Increased expression of tryptophan and tyrosine tRNAs elevates stop codon readthrough of reporter systems in human cell lines. *Nucleic Acids Res.*, **49**, 5202–5215.
72. Albers,S., Beckert,B., Matthies,M.C., Mandava,C.S., Schuster,R., Seuring,C., Riedner,M., Sanyal,S., Torda,A.E., Wilson,D.N. *et al.* (2021) Repurposing tRNAs for nonsense suppression. *Nat. Commun.*, **12**, 3850.
73. Welch,E.M., Barton,E.R., Zhuo,J., Tomizawa,Y., Friesen,W.J., Trifillis,P., Paushkin,S., Patel,M., Trotta,C.R., Hwang,S. *et al.* (2007) PTC124 targets genetic disorders caused by nonsense mutations. *Nature*, **447**, 87–91.
74. Liang,F., Shang,H., Jordan,N.J., Wong,E., Mercadante,D., Saltz,J., Mahiou,J., Bihler,H.J. and Mense,M. (2017) High-throughput screening for readthrough modulators of CFTR PTC mutations. *SLAS Technol*, **22**, 315–324.
75. de la Torre,D. and Chin,J.W. (2021) Reprogramming the genetic code. *Nat. Rev. Genet.*, **22**, 169–184.
76. Rovner,A.J., Haimovich,A.D., Katz,S.R., Li,Z., Grome,M.W., Gassaway,B.M., Amiram,M., Patel,J.R., Gallagher,R.R., Rinehart,J. *et al.* (2015) Recoded organisms engineered to depend on synthetic amino acids. *Nature*, **518**, 89–93.
77. O'Donoghue,P., Ling,J., Wang,Y.S. and Söll,D. (2013) Upgrading protein synthesis for synthetic biology. *Nat. Chem. Biol.*, **9**, 594–598.
78. Kramer,E.B., Vallabhaneni,H., Mayer,L.M. and Farabaugh,P.J. (2010) A comprehensive analysis of translational missense errors in the yeast *Saccharomyces cerevisiae*. *RNA*, **16**, 1797–1808.
79. Kuhlenkoetter,S., Wintermeyer,W. and Rodnina,M.V. (2011) Different substrate-dependent transition states in the active site of the ribosome. *Nature*, **476**, 351–354.
80. Shaw,J.J., Trobro,S., He,S.L., Aqvist,J. and Green,R. (2012) A role for the 2' OH of peptidyl-tRNA substrate in peptide release on the ribosome revealed through RF-mediated rescue. *Chem. Biol.*, **19**, 983–993.
81. McDonough,K.A. and Rodriguez,A. (2011) The myriad roles of cyclic AMP in microbial pathogens: from signal to sword. *Nat. Rev. Micro.*, **10**, 27–38.
82. Wu,C., Mori,M., Abele,M., Banaei-Esfahani,A., Zhang,Z., Okano,H., Aebersold,R., Ludwig,C. and Hwa,T. (2023) Enzyme expression kinetics by *Escherichia coli* during transition from rich to minimal media depends on proteome reserves. *Nat. Microbiol.*, **8**, 347–359.
83. Sanchez,A. and Golding,I. (2013) Genetic determinants and cellular constraints in noisy gene expression. *Science*, **342**, 1188–1193.
84. Ackermann,M. (2015) A functional perspective on phenotypic heterogeneity in microorganisms. *Nat. Rev. Micro.*, **13**, 497–508.
85. Gomes,A.C., Kordala,A.J., Strack,R., Wang,X., Geslain,R., Delaney,K., Clark,W.C., Keenan,R. and Pan,T. (2016) A dual fluorescent reporter for the investigation of methionine mistranslation in live cells. *RNA*, **22**, 467–476.
86. Rozik,P., Szabla,R., Lant,J.T., Kiri,R., Wright,D.E., Junop,M. and O'Donoghue,P. (2022) A novel fluorescent reporter sensitive to serine mis-incorporation. *RNA Biol.*, **19**, 221–233.